



Design and Simulation of a Single Unit Heliostat

S. S. Yaru

Department of Mechanical Engineering
The Federal University of Technology, Akure, Nigeria
ssyaru@futa.edu.ng

ABSTRACT

This research is aimed at to designing and simulating a single-unit heliostat, and develop a predictive model with a graphical user interface. Helioclim-3 was used to generate data for the different tilt angles for the study period, 1st to 31st January, 2021, while ray tracing was done in SolTrace. The results showed that the minimum and maximum values obtained for first principal stress was between (-0.460663 MPa and 7.27999 MPa), third principal stress (-7.64905 MPa - 0.605841 MPa), displacement (0 mm - 20.39 mm), safety (4.93108 ul - 15 ul) and equivalent strain (0 ul - 0.0000908046 ul). Von Mises stress value range was (0 MPa - 6.69225 MPa). The result shows that the maximum Von Mises is greater than the tension 0.32 kN, which confirmed that the material will not yield. The radial extent of the heliostat focal spot flux levels at a radius of about 0.35 m. Minimum and peak flux value are 14.42 and 105.739 respectively which shows that flux levels were under predicted by about 50%. It was observed that the highest sun ray reflected was 304o, this was obtained in January 30th, 2021, while the lowest was 173o obtained at 31st January, 2021. The model developed can be used to navigates the design space for all tilt angle, having predicted coefficient of determination (R^2) of 0.8690, which is not as close to the Adjusted R^2 of 0.3781. The validation of the model gave R^2 value of 0.9001. Graphic user interface was generated to calculate irradiance

Keywords: Heliostat, solar energy, Simulation, Inventor, Helioclim-3, Stress analysis

INTRODUCTION

The use of fossil fuels has discharged large quantities of air pollutant into the atmosphere due to the release of harmful gases during the burning of these fuels as combustion by-products. Also, increasing levels of carbon dioxide in the atmosphere from fossil fuel burning is believed by researchers to be the principal source of global warming over the past 150 years (Sukhatme and Nayak, 2008). They also added that power plants often discharge large amounts of waste heat to the environment. This can lead to thermal pollution in rivers and lakes thus causing harm to many forms of plant and animal lives. As a result, it has become increasingly apparent that a continued reliance on dangerously high carbon-emitting energy resources (such as fossil fuel, gas and coal), would ultimately prove to be catastrophic for the earth planet and all its inhabitants. Also, when examined in light of their “depleting” feature, these conventional energy resources seem to fall short of the standard in meeting the growing energy demands of both the present and the future and this does not make the environment safe. To this end, implementing a shift in the current approach of generating energy has been lauded by scholars, policy experts and organizations as one of the grand challenges facing the planet today (Jia et al., 2019). Steam generation with fire wood also leads to soot-contaminated air, food, and water, which is harmful to health (Ochsner et al., 2015). A great amount of solar radiation with high intensity is incident on the tropical region of the earth where Nigeria is located. Therefore, many applications of renewable energy with the sun being the source can be obtained such as heating, and steam production (Philibert, 2005, Burgess et al., 2009). The aim of this research is to design and simulate heliostat for steam generation. The specific objectives of the research are to design heliostat simulate the designed heliostat; and develop a regression predictive model to evaluate its performance. More recently, a few studies investigated specifically the dynamic wind loads on heliostats. Huss et al. (2011) performed aeroelastic measurements of a 14.4 m² heliostat that was used in a commercial power plant. Griffith et al. (2011) investigated a 37 m² U-shaped heliostat structure, and conducted numerical and experimental modal analysis to determine the dynamic properties and validate their finite element model. Later, Ho et al. (2012) carried out operational modal analysis (OMA) on the

same heliostat to examine the dynamic behaviour of the structure under real operating conditions. They found that the natural frequencies determined under windy conditions were in very close agreement to the previous study, and that the aerodynamic damping is very small under these conditions. In the work by Ghanadi et al. (2016) an unsteady computational fluid dynamic model was used to estimate the peak and mean drag coefficients for a heliostat installed perpendicular to the flow neglecting dynamic effects. For 18% turbulence intensity the variation in amplitude of load can be already without the dynamic content equivalent to the mean load, which corresponds to the values measured by Peterka and Derickson (1992) with stiff models (i.e. also excluding the impact of dynamic properties).

METHODOLOGY

Field Size

The field that was used for this project is 10 m x 5 m, rectangular plot within the University community located at the back of school of Mechanical Engineering workshop building.

Design Considerations

The following were considered; tower height, number of heliostats, location and accessibility to solar radiation and Cosine losses of heliostat relative to the receiver.

Design Analysis

Structural deflection

A rough estimation of the wind forces acting on the structure is obtained by simply calculating the dynamic pressure using equation (1) by Okeniyi et al. (2015):

$$q = \frac{1}{2} \rho v^2 \quad (1)$$

where q is dynamic pressure (Pa); ρ is density of air (1.23 kg/m^3); v is wind speed (m/s) the maximum wind speed of Akure ranges between 1.24 and 4.24 m/s (Okeniyi *et al.*, 2015), for this calculation 5 m/s was used for optimum design. Equation (2) is for a mirror surface placed perpendicular to the wind flow; that is the pressure is acting normal on the mirrors (either in front side or backside).

Calculating the dynamic pressure:

$$q = \frac{1}{2} 1.23 \times 5^2 = 15.38 \text{ N/m}^2 \quad (2)$$

Since $1 \text{ Pa} = 1 \text{ N/m}^2$, the wind force F on the array, when positioned perpendicular to the wind flow as shown in Figure 3.1, equation (3.3) was used to calculate this force acting on a single facet;

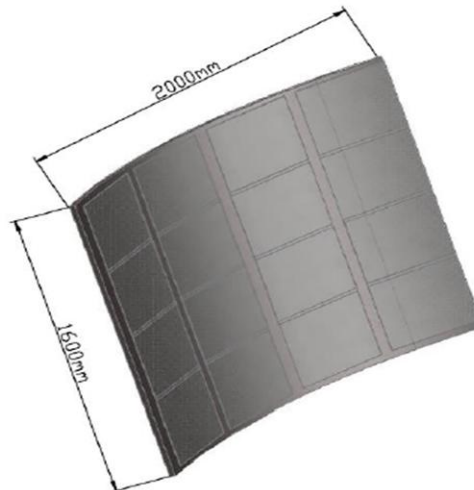


Figure 1: Facet dimension

$$F = q \times A \quad (3)$$

$$F = 15.38 \times (2 \times 1.6)$$

$$F = 49.22 \text{ N}$$

where A is the area of the mirror array (m^2) i.e length x breath, $l=2$, $b= 1.6$.

The resulting moment was obtained by multiplying the force F with the moment arm of the heliostat (Peterka, 1992); as shown in Figure 2

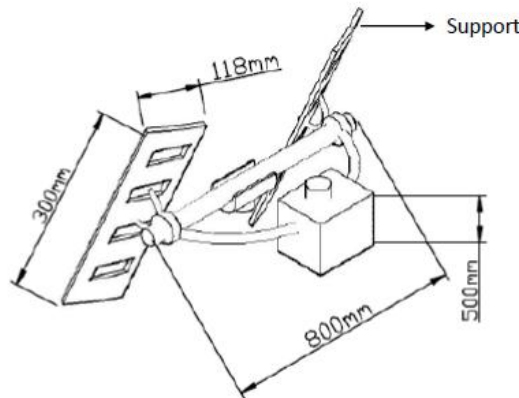


Figure 2: Rotor unit showing the moment arm

$$M = F \times r$$

$$M = 49.22 \times 0.8$$

$$M = 39.37 \text{ Nm}$$

The following assumptions were made for the design

- (i) Rectangular shaped mirror was used on the facet
- (ii) Forces on the binds are neglected
- (iii) The pedestal area is neglected.

Wind load calculation

Table 1 shows the K-factor which was reported by Kolb (2014) for wind loading of a rectangular shape heliostat with rectangular shaped mirror fitted to the facet

Table 1: K-factor for spherical shape heliostat with rectangular shaped mirror fitted

k-Factors	
	K
F_x	4
F_z	1

(Kolb, 2014)

Therefore, the drag force acting on the heliostat was calculated using equation (4) (Kolb, 2014);

$$\text{Drag force} = F_x = CF_x \times q \times A \tag{4}$$

$$\text{Lift force} = F_z = CF_z \times q \times A$$

where:

A is actual surface area of the heliostat mirror-array (m²)

q is Mean dynamic Pressure N/m²

CF_x is from the k- factor table

CF_z is from the k-factor table.

$$\begin{aligned} \text{Drag force} &= F_x = CF_x \times Q \times A \\ &= 4.0 \times 15.38 \times 3.2 \\ &= 196.86 \text{ N} \end{aligned}$$

$$\begin{aligned} \text{Lift force} &= F_z = CF_z \times Q \times A \\ &= 1.0 \times 15.38 \times 0.332 \\ &= 5.1 \text{ N} \end{aligned}$$

Characteristic Diameter

The characteristic diameter is the distance between the center of the adjacent heliostats, and it can be calculated using equation 5 by Kolb (2014);

$$DM = \sqrt{(l_w)^2 + (l_h)^2} \tag{5}$$

where DM is the characteristic diameter of the heliostat in m, $l_w = 2 \text{ m}$ and $l_h = 1.6 \text{ m}$ are the width and height of the heliostat facet in m.

Substituting into the above equation;

$$\begin{aligned} DM &= \sqrt{(2)^2 + (1.6)^2} \\ DM &= 2.56 \text{ m} \end{aligned}$$

The Radial and Azimuth Spacing

The minimum radius of the heliostats should ensure that adjacent heliostats do not allow mechanical collisions.

$$\Delta R_{min} = DM \times \cos 30^\circ \quad (\text{Peterka, 1992}) \quad (6)$$

Based on the number of heliostats in each row of the first zone, radial distance from the tower to the first row of the heliostats (R_1) can be calculated using equation (7)

$$R_1 = N_{hel_1} \frac{DM}{2\pi} \quad (7)$$

Where N_{hel_1} is the number of heliostats within each row of the first zone (in this case 1 is the heliostat number) DM is 2.21 m

Solar position

The solar position is very important because the sun is changing hourly during a day at 15° every hour and daily during the year, so it is necessary to know the solar coordinate systems during the year through solar hour angles (ω), zenith angle θ_z , azimuth angle γ_s , celestial declination δ_s and solar altitude α_s , before continuing, let the meaning of solar altitude α_s , zenith angle θ_z , azimuth angle γ_s and hour angle ω be known. The solar altitude is measured in degrees from horizon of the projection of the radiation beam to the position of the sun (when the sun is overhead, $\alpha_s = 90^\circ$ and when the sun is over the horizon, $\alpha_s = 0^\circ$). Whereas, zenith angle is the angle of the sun relative to a line perpendicular to the earth's surface. The meaning of solar azimuth is the angle on the horizontal plane between the projection of the beam radiation and the north-south direction line ($+\gamma_s =$ the sun is west of south and $-\gamma_s =$ the sun is east of south). The hour angle, which is defined as angular distance between the sun's position at a particular time and its highest position for that day when crossing the local meridian at the solar noon

Table 2: Time factor and hour angle ω for respective times

Time	Time Factor	Hour Angle ω
7 a.m.	-5	$-5 \times 15^\circ = -75^\circ$
8 a.m.	-4	$-4 \times 15^\circ = -60^\circ$
9 a.m.	-3	$-3 \times 15^\circ = -45^\circ$
10 a.m.	-2	$-2 \times 15^\circ = -30^\circ$
11 a.m.	-1	$-1 \times 15^\circ = -15^\circ$
12 noon	0	$0 \times 15^\circ = 0^\circ$
1 p.m.	+1	$+1 \times 15^\circ = +15^\circ$
2 p.m.	+2	$+2 \times 15^\circ = +30^\circ$
3 p.m.	+3	$+3 \times 15^\circ = +45^\circ$
4 p.m.	+4	$+4 \times 15^\circ = +60^\circ$
5 p.m.	+5	$+5 \times 15^\circ = +75^\circ$
6 p.m.	+6	$+6 \times 15^\circ = +90^\circ$
7 p.m.	+7	$+7 \times 15^\circ = +105^\circ$

Table 2 is the calculation of solar hour angle, at solar noon (local meridian), the value of the hour angle is zero and takes negative values during mornings and positive values in the afternoons. In other words, the time representatives or time factor from 7 a.m. to 7 p.m. are listed.

The solar declination is calculated by (8):

$$\delta_s = 23.45 \sin \frac{360}{365} (284 + N) \quad (8)$$

where N is the number of days during the year starting from the 1st of January

The solar altitude angle α_s is calculated by equation (9) by Kolb (2014);

$$\sin \alpha_s \sin \phi \sin \delta + \cos \alpha \cos \phi \cos \delta \quad (9)$$

where α , ϕ and δ are;

latitude, declination and angular hour respectively,

And since $\sin^2 \alpha_s + \cos^2 \alpha_s = 1$;

$$\cos \alpha_s = (1 - \sin^2 \alpha_s)^{1/2} \quad (10)$$

Substituting into equations (11)

$$\sin \alpha_s = \sin 7.20 \sin 15.36 + \cos 7.20 \cos 15.36 \cos \omega$$

$$\sin \alpha_s = 0.5114$$

$$\text{since } \sin^2 \alpha_s + \cos^2 \alpha_s = 1 \text{ } \cos \alpha_s = (1 - 0.5114^2)^{1/2} \text{ } \cos \alpha_s = 0.6989$$

$$\cos \alpha_s = \left(\frac{\sin \alpha_s}{\cos \alpha_s} \right), \cos \alpha_s = 0.7317 \quad (11)$$

$$\alpha_s = 42.97^\circ$$

The cosine component of zenith angle θ_z can be calculated using equation (10);

$$\cos \theta_z = \sin \phi \sin \delta + \cos \phi \cos \delta \cos \omega$$

$$\cos \theta_z = \sin 7.20 \sin 15.36 + \cos 7.20 \cos 15.36 \cos 60$$

$$\theta_z = 0.$$

And since $\sin^2 \alpha_s + \cos^2 \alpha_s = 1$;

$$\cos \alpha_s = (1 - \sin^2 \alpha_s)^{1/2}$$

$$\alpha_s = \tan^{-1} \left(\frac{\sin \alpha_s}{\cos \alpha_s} \right)$$

Substituting into equations

$$\sin \alpha_s = \sin 7.20 \sin 15.36 + \cos 7.20 \cos 15.36 \cos 60$$

$$\sin \alpha_s = 0.5114$$

since $\sin^2 \alpha_s + \cos^2 \alpha_s = 1$

$$\cos \alpha_s = (1 - 0.5114)^{1/2}$$

$$\cos \alpha_s = 0.6989$$

$$\cos \alpha_s = \arctan \left(\frac{\sin \alpha_s}{\cos \alpha_s} \right) \tag{12}$$

$$\cos \alpha_s = 0.7317$$

$$\alpha = 42.97^\circ$$

The cosine component of zenith angle θ_z can be calculated using equation (13).

$$\cos \theta_z = \sin \phi \sin \delta + \cos \phi \cos \delta \cos \omega \tag{13}$$

$$\cos \theta_z = \sin 7.20 \sin 15.36 + \cos 7.20 \cos 15.36 \cos 60$$

$$\cos \theta_z = 0.5114$$

$$\theta_z = 59.24^\circ$$

The azimuth angle is calculated using equation (14);

$$\gamma_s = \arctan \left(\frac{\sin \omega \cos \theta}{\sin \theta} \right) \tag{14}$$

Substituting the value of hour angle, declination angle and zenith angle into the above equation.

$$\gamma_s = 76.33^\circ$$

Heliostat position

The solar altitude angle of the tower receiver for each heliostat (α_{tr}) which is defined by the tower height (H_t), the height of heliostat (H_h) and the distance of the heliostat from the tower base (R) is calculated.

where (H_t) = 8.6 m, (H_h) = 2.9 m and (R) = 6 m

$$\alpha_{tr} = \tan^{-1} \frac{H_t - H_h}{R} \tag{15}$$

substituting the values of (H_t), (H_h) and (R) into the equation (15);

$$\alpha_{tr} = 43.53^\circ$$

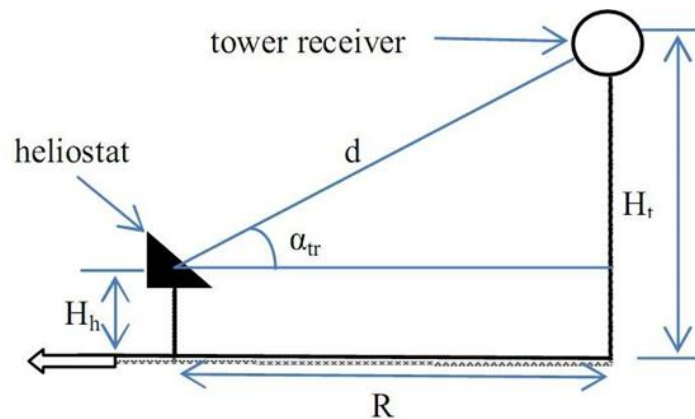


Figure 3: Solar altitude angle of tower receiver

For calculating the distance of each heliostat from the tower receiver (d), the Pythagorean Theorem is used.

Where (H_t) = 8.6 m, (H_h) = 2.9 m and (R) = 6 m

$$d = \sqrt{R^2 + (H_t - H_h)^2} \tag{16}$$

Substituting into the above equation;

$$d = 8.27 \text{ m}$$

In order to reflect the incident radiation on heliostat and direct it to the tower receiver, the rotation angle was calculated using equation (3.15) by Kolb (2014);

$$\beta_{hs} = \frac{\alpha_{tr} + \alpha_s}{2}$$

where, $\alpha_{tr} = 43.53^\circ$ $\alpha_s = 42.9^\circ$

$$\beta_{hs} = 26.310$$

The solar incidence angle on each heliostat (θ_s) is calculated using equation (3.16) by Kolb (2014);

$$\theta_s = \cos^{-1} \left[\begin{aligned} &(\sin \phi_{lat} \times \sin \delta_s \times \cos \beta_{hs}) - (\cos \phi_{lat} \times \sin \delta_s \times \sin \beta_{hs} \times \cos \phi_{surface}) + (\cos \phi_{lat} \times \cos \delta_s \times \cosh_s \times \cos \beta_{hs}) \\ &+ (\sin \phi_{lat} \times \cos \delta_s \times \cosh_s \times \sin \beta_{hs} \times \cos \phi_{surface}) + (\cos \delta_s \times \sinh_s \times \sin \beta_{hs} \times \sin \phi_{surface}) \end{aligned} \right] \tag{17}$$

where, $\phi_{lat} = 7.2^\circ$, $\delta_s = 15.36^\circ$, $\beta_{hs} = 43.21^\circ$, $h_s = 15^\circ$ and $\phi_{surf} = 1$

$$\theta_s = \cos^{-1} (0.862)$$

$$\theta_s = 26.25^\circ$$

Solar Radiation

For modelling the incident radiation on the tower receiver , it is mandatory to calculate the extraterrestrial radiation(G_o),the beam irradiance normal to the solar beam (B_{oc}) and the solar beam irradiation on an inclined surface (B_{ic}), and to define the linked atmospheric turbidity factor (Tlk), the relative optical air mass (m_{opt}) and the Rayleigh optical thickness at air mass(d_{rm}).The extraterrestrial radiation normal to the solar beam (G_o) is computed as a function of the solar constant($G_{sc}=1367 \text{ W.m}^{-2}$) (Hnin and Nang, 2017),

$$G_o = G_o = G_{sc} (1 + 0.033 \cos \frac{360N}{365}) \cos \theta_z \tag{18}$$

where θ_z is the solar zenith angle previously calculated as 59.24° and N is number of days = 222

Substituting into equation (18);

$$G_o = 1349 \text{ W.m}^{-2}$$

The beam irradiance normal to the solar beam (B_{oc}) is calculated through equation

$$B_{oc} = G_o \cdot \exp(-0.8662 \cdot \text{Tlk} \cdot m_{opt} \cdot d_{rm}) \tag{19}$$

Where Tlk = 0.2, $m_{opt} = 0.99$, $d_{rm} = 0.093$, $G_o = 1349 \text{ W.m}^{-2}$

$$B_{oc} = 139 \text{ Wm}$$

For putting the relative optical air mass (m_{opt}), a condition for solar altitude angle (α_s) is used:

$$\text{If } \alpha_s > 30^\circ, m_{opt} = \frac{1}{\sin \alpha_s} \tag{20}$$

Else $\alpha_s < 30^\circ$, Since α_s is greater than 30° therefore,

$$m_{opt} = 0.99$$

The Rayleigh optical thickness at air mass (d_{rm}) is obtained with two empirical equations

$$d_{rm} = \frac{1}{10.04 + 0.718 M_{opt}} \tag{21}$$

Substituting $M_{opt} = 0.99$

$$d_{rm} = 0.0093 \text{ kg}$$

The solar beam irradiation on an inclined surface (B_{ic}) is given in equation (22);

$$B_{ic} = B_{oc} \sin \theta_s \tag{22}$$

Where $B_{oc} = 139$ and $\theta_s = 26.25^\circ$

$$B_{ic} = 139 \times \sin 26.25$$

$$B_{ic} = 61.48 \text{ Wh/m}$$

After obtaining the value of irradiation for one year and for each heliostat, the solar thermal power received at the tower receiver (Q_{tr})

$$Q_{tr} = B_{ic} \times A_{hs} \times \eta_{opt} \tag{23}$$

where, A_{hs} is area of the receiver aperture, η_{opt} is optical coefficient of the mirror

$$Q_{tr} = 61.48 \times 3.142 \times 0.05^2 \times 0.98$$

$$Q_{tr} = 4.6 \text{ Wh}$$

The solar power received by the receiver is high enough to keep the molten salt in receiver chamber in liquid state which water passes through gives a rapid steam at the outlet chamber.

Maximum allowable deflection

The maximum allowable wind load deflection is defined by the Sandia requirements as 3.6 mrad root mean square (RMS) on the reflective surface (Kolb, 2007), which is a requirement for obtaining appropriate optical accuracy during normal operation.

RMS, Root Mean Square:

If n is a set of values $\{x_1, x_2, \dots, x_n\}$, then the RMS-value is given by:

$$x = \sqrt{1 (X^2_1 + X^2_2 + \dots + X^2_n)} \tag{24}$$

rsm= n, 1, 2,3n

The simplest interpretation is that the mirror array, seen from side view in 2D, consist of two rigid links that rotate symmetrical around the centre hinge when a large wind force is applied. Since deformations are small, the change of point p’s position at the y-axis after bending is neglected in the analysis.

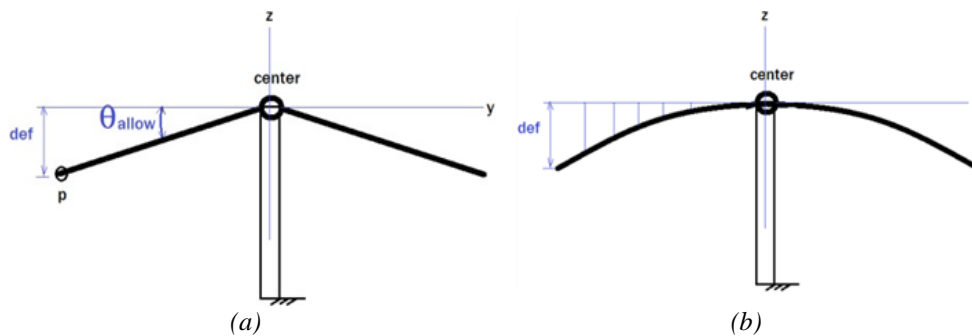


Figure 4: Wind Load deflection

(a) Simplified interpretation of the wind load deflection requirement, (b) detailed interpretation of the wind load requirement.

The triangular relationship (Figure 4) holds that;

$$\tan (\theta_{allow}) = \frac{def}{h} \tag{25}$$

where def = maximum deflection.

h = distance between the edge and the centre point

theta_allow is degree of direction, where h is the distance between the edge and the center point.

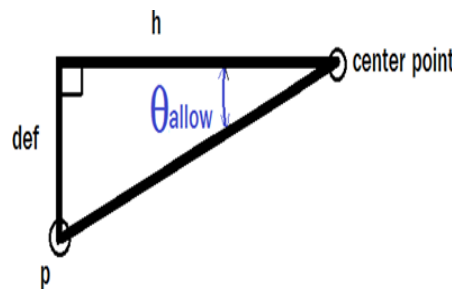


Figure 5: Angle direction

To find maximum allowed deflection from a triangular relationship

The maximum deflection def [m] allowed at the edge of the mirror array is:

$$def = 1 \times \tan (\theta_{allow})$$

where 1 is half of the length of heliostat facet

$$def = 1 \times \tan 30$$

$$def = 0.57m$$

The maximum deflection def [m] allowed at the centre of the mirror array is:

Using Pythagoras theorem from figure 26

$$X^2 = h^2 + def^2 = 1^2 + 0.57^2 = 1.33, X = 1 \tag{26}$$

Simulation

The modelling and simulation was performed using Autodesk Inventor 16 to determine stress and displacement loads on the structure, as well as to simulate the shape of the heliostat. The sun rays was traced using

SOLTRACE software to determine the flux on the receiver and heliostat facet using the latitude, heliostat distance and optical reflectivity coefficient as parameters. Then the designed heliostat was simulated on heliochim-3 software with latitude, tilted angle, azimuth angle, hourly and monthly intervals and the parameter to determine the solar hour angle the temperature will be at highest and lowest, how clear sky influence amount of rays getting to the heliostat surface and to see effect of wind speed as it affected the performance of the heliostat. Model generation for the irradiance was done using design expert 12 using a composite design. R studios was the method for visualizing multivariate data was used for the irradiance calculation.

RESULTS AND DISCUSSION

Stress strain Analysis

The summary of the simulation carried out is presented in Table 3, containing minimum and maximum values for the first principal stress, third principal stress, displacement, safety, first principal strain and third principal strain of the heliostat components. It was observed that for the volume of the heliostat was 57.8 m3 having a total mass of 326.42 kg in terms of weight and 0.32 kN in terms of tension. The minimum and maximum values obtained for first principal stress was between (-0.460663 MPa and 7.27999 Mpa), third principal stress (-7.64905 Mpa-0.605841 Mpa), displacement (0 mm-20.39 mm), safety (4.93108 ul-15 ul) and equivalent strain (0 ul-0.0000908046 ul). The Von Mises stress value range was (0 Mpa-6.69225 Mpa), which was used to determine yield strength for the given material (galvanized steel). The result shows that the maximum Von Mises is greater than the tension 0.32 kN. This means the yield criteria for maximum principal stress, Von Mises stress, displacement, safety factor etc to define failure is a good criterion which worked better in the heliostat design for stress level, under load condition, at any point. The heliostat is limited to a level that provides a maximum safety factor of 15 ul against permanent deformation which is purely static strength criterion, which agrees with Capecchi and Ruta (2015) that this means limit load is 1/15th of the yield stress for the heliostat, therefore, any range above the safety level under will cause crack or deformation, this agree with (Capecchi and Ruta, 2015) that if the Von Mises stress of a material under load is equal or greater than the yield limit of the same material under simple tension, then the material will yield.

Figures 7-10 show the single unit stress analysis for frame, facet, rotor unit and tower

Table 3: Result Summary for the simulation of the Heliostat

Name	Minimum	Maximum
Volume	57823500 mm ³	
Mass	326.417 kg	
Von Mises Stress	0 Mpa	6.69225 Mpa
1 st Principal Stress	-0.460663 Mpa	7.27999 Mpa
3 rd Principal Stress	-7.64905 Mpa	0.605841 Mpa
Displacement	0 mm	20.3939 mm
Safety Factor	4.93108 ul	15 ul
Equivalent Strain	0 ul	0.0000908046 ul
1 st Principal Strain	-0.000000172566 ul	0.0000976349 ul
3 rd Principal Strain	-0.000104014 ul	0.00000153873 ul

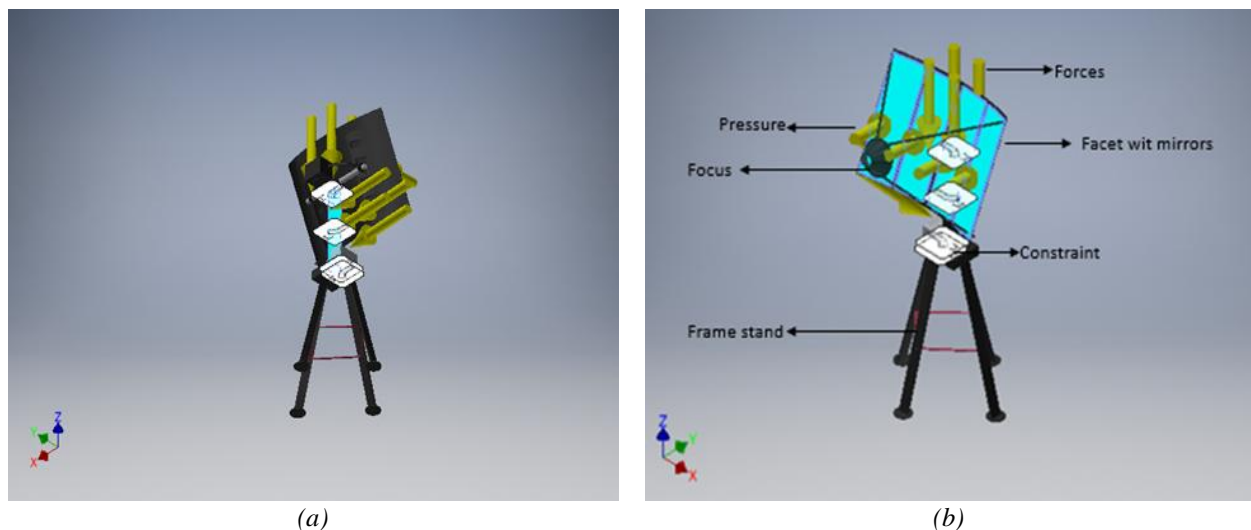


Figure 6: Forces and pressure acting on the faces of the heliostat (a) back view and (b) front view

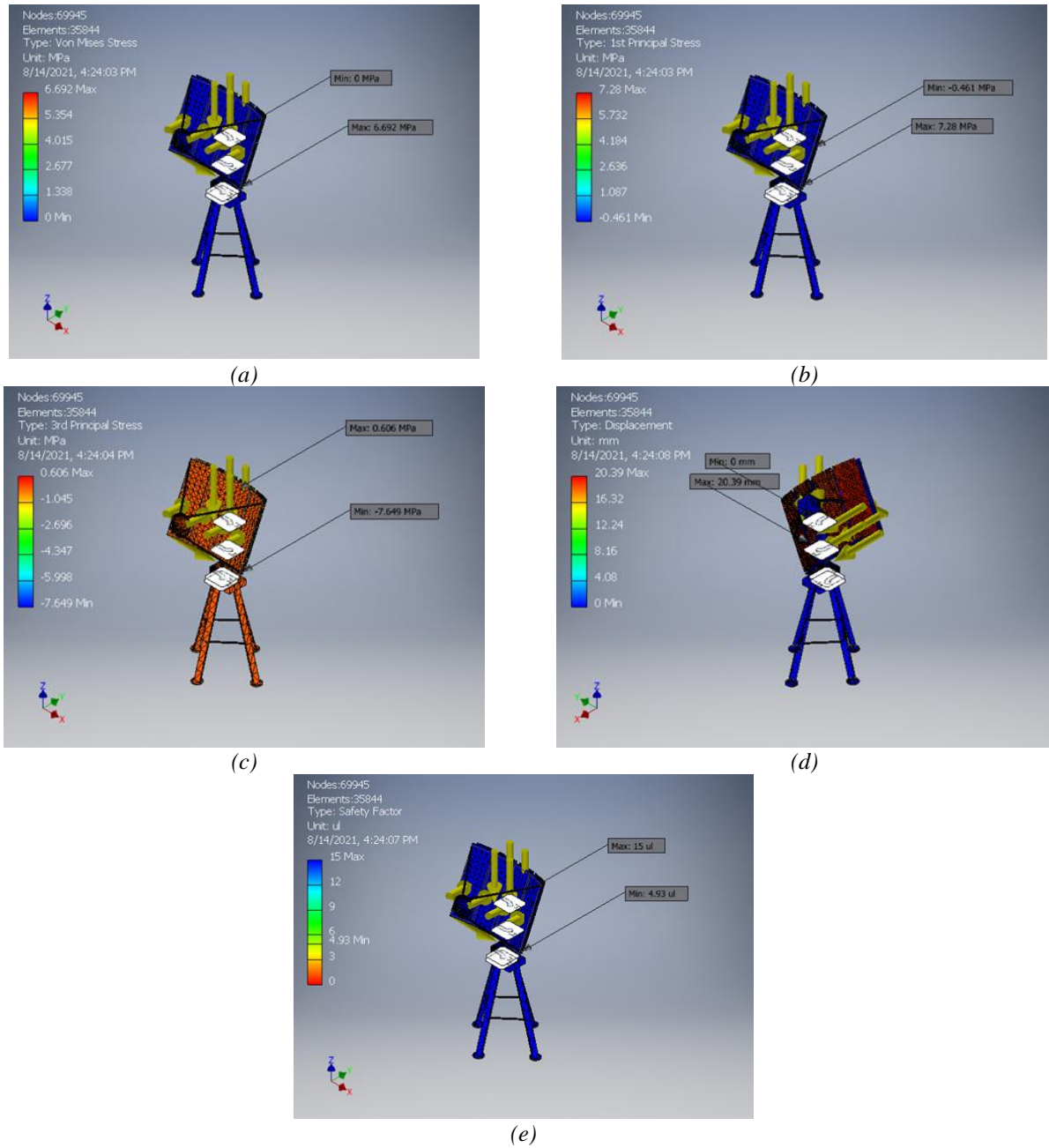
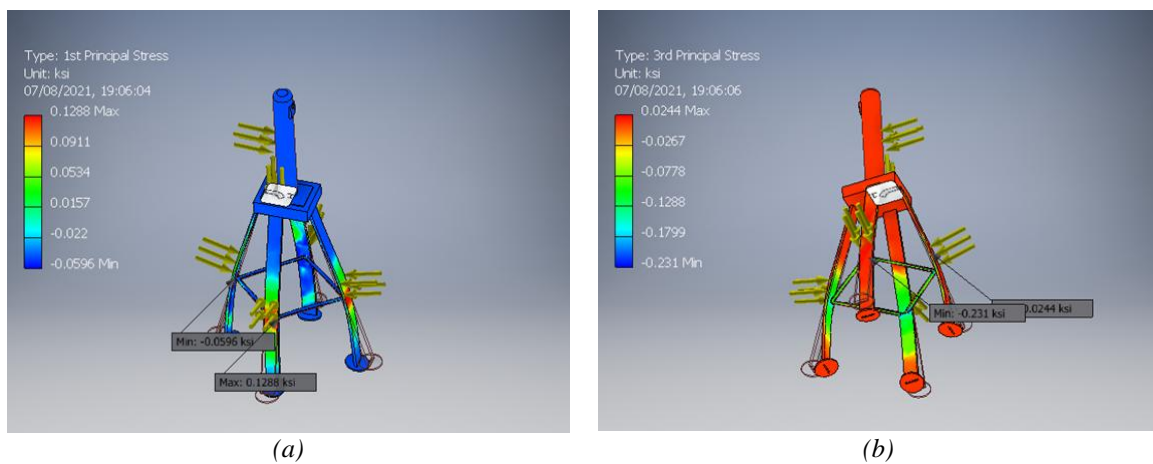
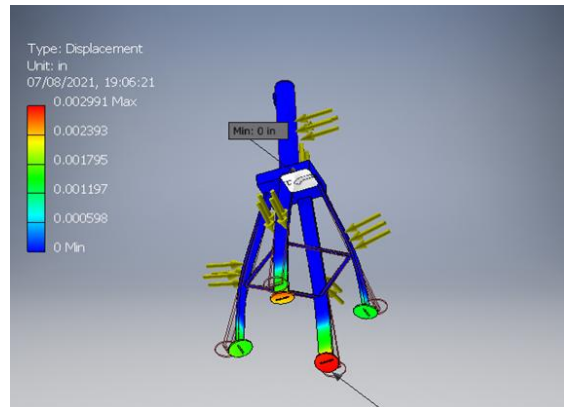


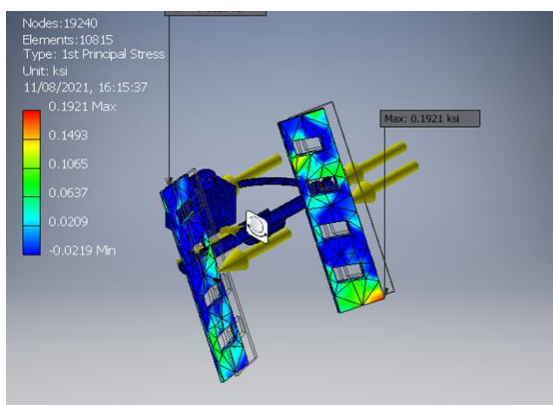
Figure 7: (a) Von mess stress (b) 1st principal stress (c) 3rd principal stress (d) displacement and (e) safety factor



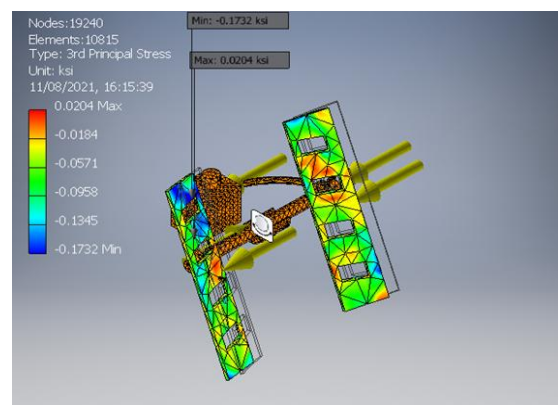


(c)

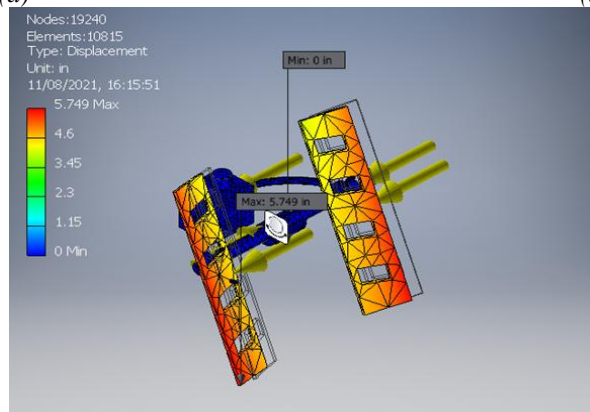
Figure 8: a) First principal b) third principal c) displacement stress analysis on frame support



(a)

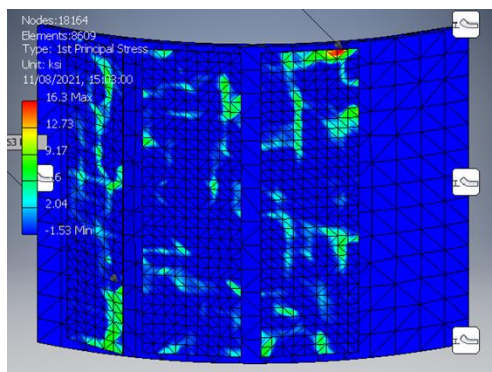


(b)

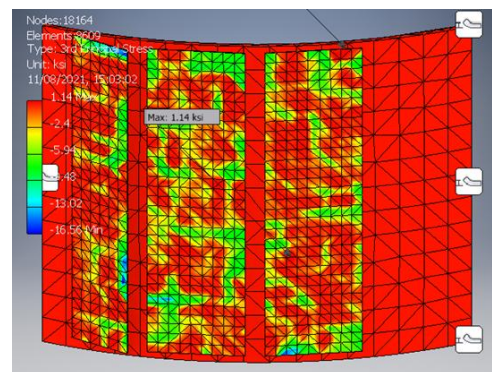


(c)

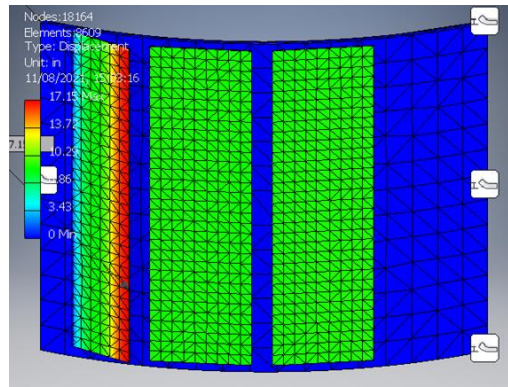
Figure 9: a) First principal b) third principal c) displacement stress analysis on rotor mechanism



(a)

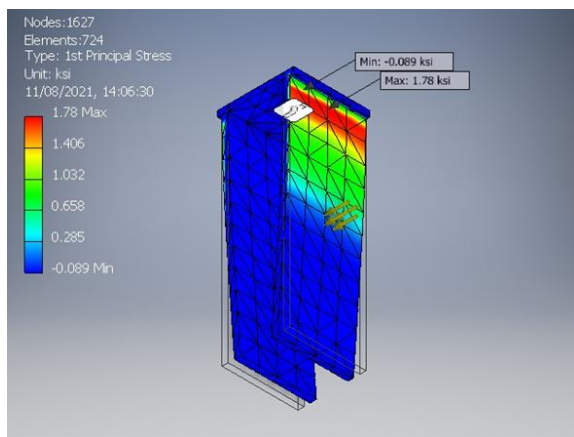


(b)

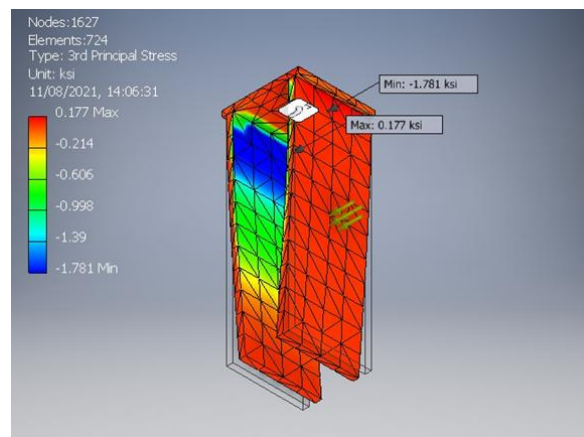


(c)

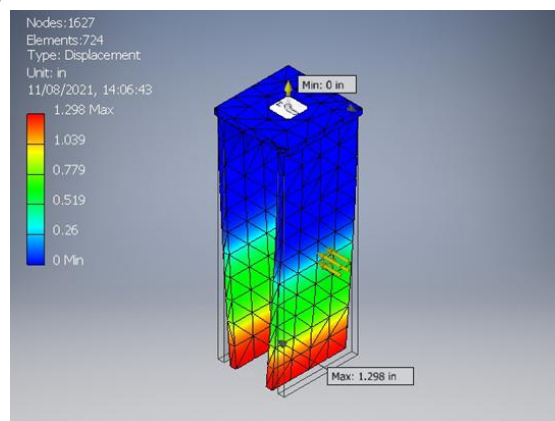
Figure 10: a) First principal b) third principal c) displacement stress analysis on facet



(a)



(b)



(c)

Figure 11: a) First principal b) third principal c) displacement stress analysis on Tower

Ray Tracing Simulation

Measurements of flux distributions of the designed heliostats simulated on Soltrace gives deflectometry measurement accuracy and the ray tracing model by comparison having sun ray count of 384,081. In order to take into account as many influences as possible, the heliostats parameters inputted gave lines of flux has shown in Figure 11 having 107.8 power per ray.

Figure 12 shows a screenshot from a SolTrace simulation. On the far left are icons to open windows for different stages in the creation and execution of a ray-tracing simulation, the results are presented on the right which shows a view of a three-dimensional ray tracing simulation. The positive y-direction is vertical, the positive x-direction is due east and the view into the page is due north. Individual rays (yellow lines) are shown, traced downward from the sun (at approximately 45°), reflecting off the mini heliostat panels (bottom right of white grid) upward to beam-down mirror (top left of grid), and finally reflected vertically downward into the receiver. Figure 13 shows the measured flux distribution of the heliostats (bold lines) and the ray tracing result (thin lines) in an overlay which

shows that agreement between both distributions is very good which means that local surface deviations, as well as shading and blocking are correctly reflected in measurement and simulation. The radial extent of the heliostat focal spot appears to be relatively well predicted, with ray-tracing predictions agreeing with experimental flux levels at a radius of about 0.35 m. The shape of the flux distribution also appears to be well captured, resembling a Gaussian distribution. The minimum and peak flux value are 14.42 – 105.74, this shows that flux levels was under predicted by about 50%, however, this type of highly accurate ray tracing simulations based on high resolution measurement data allows much more realistic predictions and optimizations of the heliostat field performance than pillbox and user-defined profiles simulation models, which agrees with Garcia et al. (2008) that reported shape deviations of heliostats approximated with a single value for a Gaussian slope error distribution gives good flux

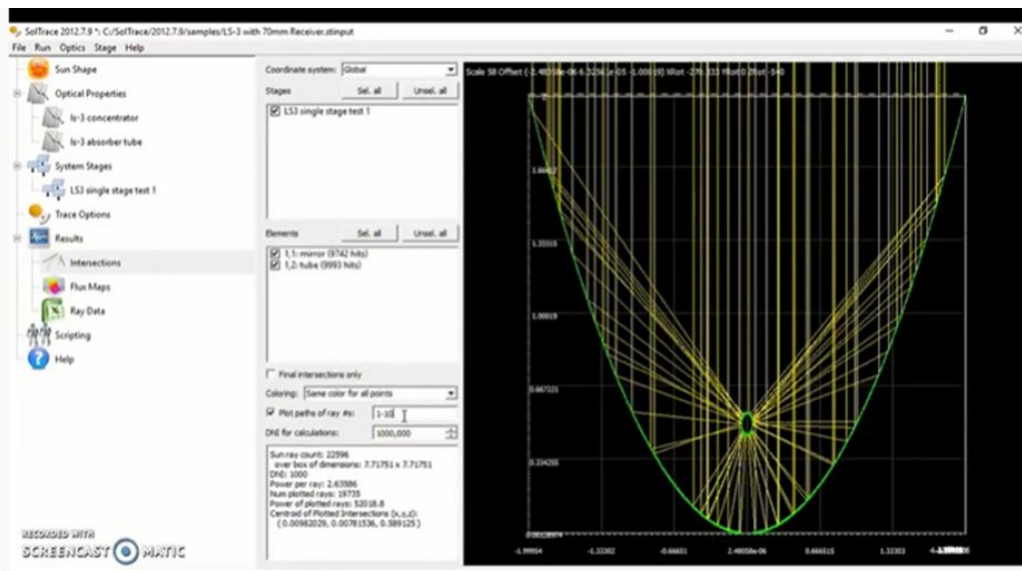


Figure 12: Screenshot of ray tracing SolTrace with heliostat set-up

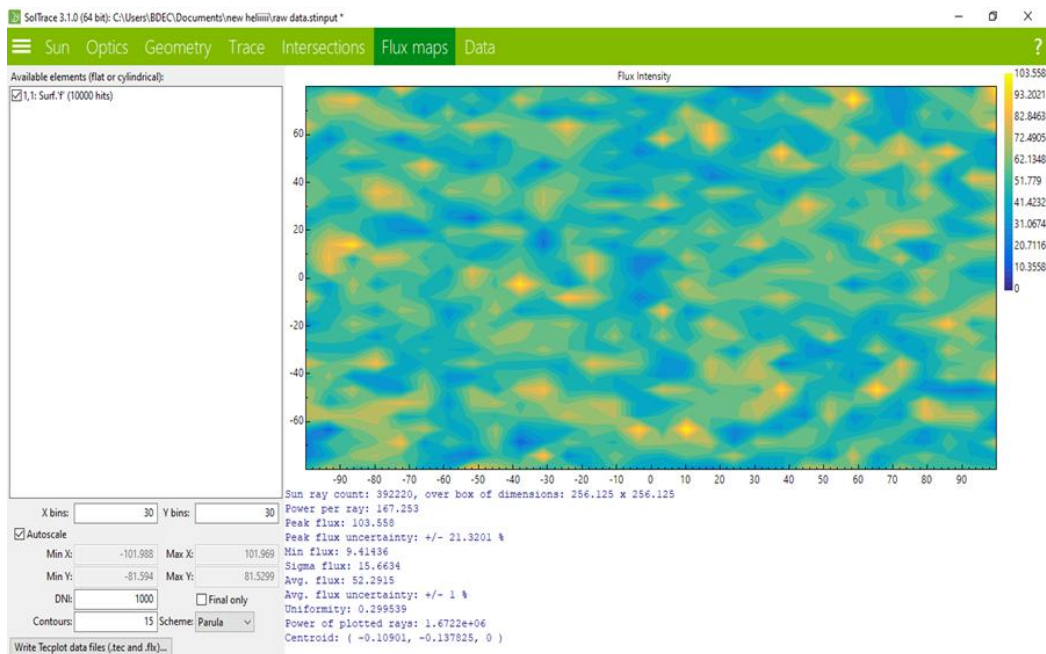


Figure 13: Measured flux distribution of the heliostats (bold lines), and simulated flux distribution of heliostats based on measured reflectometry data (thin lines)

Wind simulation for the heliostat

Table 4 shows the designed speed for the heliostat which were the drag force and lift force acting on the facet of the heliostat. The highest designed wind speed was 3.56 m/s design which was observed for the duration of experiment (wind data gotten for Akure in January, 2021). The probability density function of the horizontal wind speed data is

shown in Figure 14 together with a Weibull distribution that fits very well the measurements with a shape factor of 1.5. The daily average wind speed was 2.3 m/s while the maximum Weibull distribution density was found to be 0.25. In Figure 13 the distribution is divided into three ranges. Weak and medium wind speeds are defined within the operational conditions of heliostat fields, usually given by the maximal reference wind speed of 5 m/s. The designed speed of 5 m/s was used to simulated the facet of the heliostat at different angle of elevation 30o, 60o and 90o as shown in Figure 15. It was observed that the simulated facet responded well to the wind with no much deformation

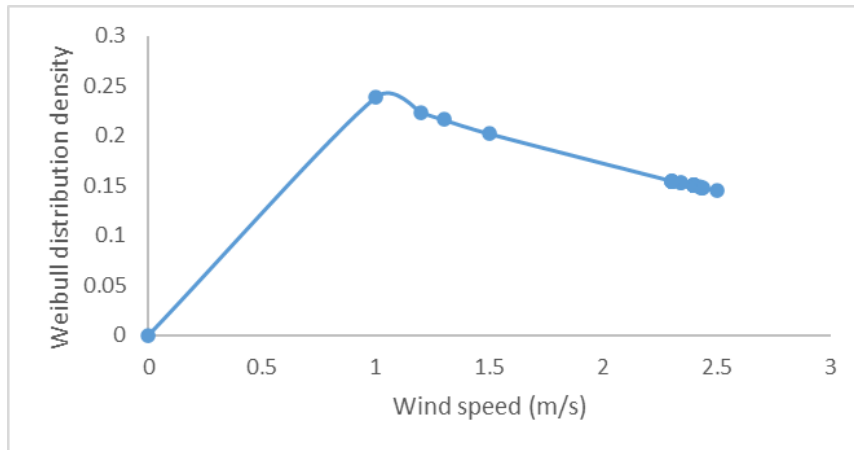


Figure 14: Weibull distribution wind speed density

Table 4: Different generated wind speed for the heliostat at different elevation angle

Days/time	30 degree Wind speed (m/s)	60 degree Wind speed(m/s)	90 degree Wind speed(m/s)
2021-01-01 00:00:00	1.41	1.41	1.41
2021-01-02 00:00:00	1.31	1.31	1.31
2021-01-03 00:00:00	1.11	1.11	1.11
2021-01-04 00:00:00	0.63	0.63	0.63
2021-01-05 00:00:00	1.18	1.18	1.18
2021-01-06 00:00:00	3.3	3.3	3.3
2021-01-07 00:00:00	3.17	3.17	3.17
2021-01-08 00:00:00	3.56	3.56	3.56
2021-01-09 00:00:00	3.25	3.25	3.25
2021-01-10 00:00:00	3.51	3.51	3.51
2021-01-11 00:00:00	3.29	3.29	3.29
2021-01-12 00:00:00	2.24	2.24	2.24
2021-01-13 00:00:00	2.03	2.03	2.03
2021-01-14 00:00:00	1.36	1.36	1.36
2021-01-15 00:00:00	0.56	0.56	0.56
2021-01-16 00:00:00	0.74	0.74	0.74
2021-01-17 00:00:00	0.04	0.04	0.04
2021-01-18 00:00:00	1.96	1.96	1.96
2021-01-19 00:00:00	1.48	1.48	1.48
2021-01-20 00:00:00	0.39	0.39	0.39
2021-01-21 00:00:00	1.84	1.84	1.84
2021-01-22 00:00:00	1.24	1.24	1.24
2021-01-23 00:00:00	1.39	1.39	1.39
2021-01-24 00:00:00	0.95	0.95	0.95
2021-01-25 00:00:00	0.6	0.6	0.6
2021-01-26 00:00:00	0.81	0.81	0.81
2021-01-27 00:00:00	2.09	2.09	2.09
2021-01-28 00:00:00	1.54	1.54	1.54
2021-01-29 00:00:00	1.78	1.78	1.78
2021-01-30 00:00:00	1.85	1.85	1.85
2021-01-31 00:00:00	2.1	2.1	2.1

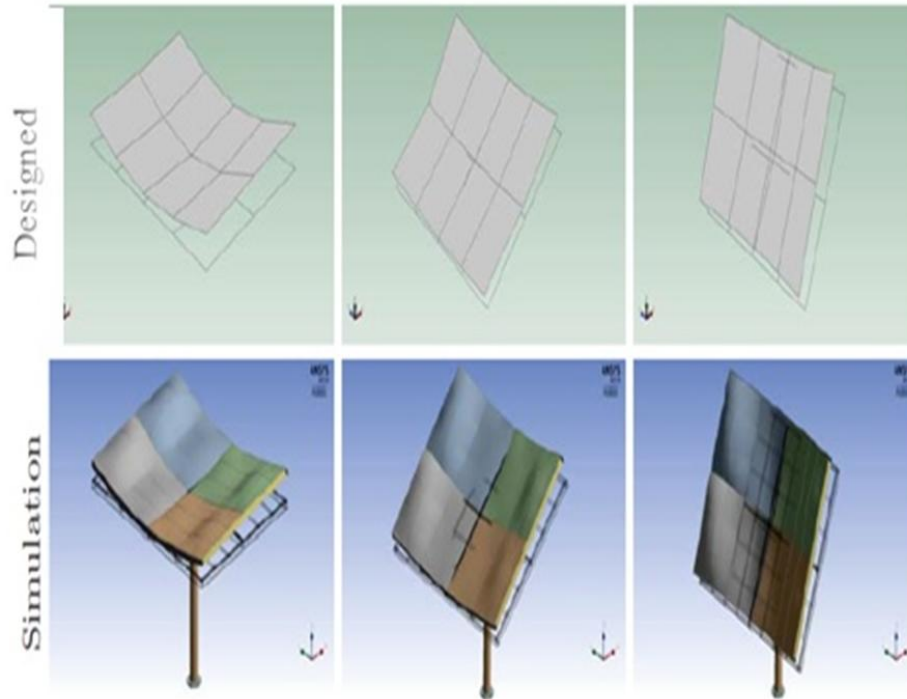


Figure 15: Comparison between Designed and simulated facet at different elevation angle (300, 600, 900)

Irradiance received by the receiver

Figure 16 shows that the highest temperature of 298.080C and reflected value 304 wh/m2 was recorded was in January, 2021 and lowest for the month of August, 2021, this gives the reason of choosing data from January, 2021 for the simulation., having abundance sun reflection which is good for our designed heliostat. The irradiance shows that data with irradiances lower than 50 [W/m2] were excluded from the analysis. For irradiance exceeding 50 [W/m2] only 3.1% of the data had an absolute relative error greater than 1 % (Rashid et al., 2021; Khodayar et al., 2021).

Figure 17 shows that the hourly reading for a day and it was observed that the sun was at the highest from 12.00-1.00 pm, this is not surprising as the sun is at the zenith angle at these hours as well the sun angular hour was very close when the sun is at the overhead. It can also be pointed out that the sky was at a clearer state which also is a factor affecting reflectivity of heliostat as radiation reaching the surface reduces when the sky is less clear. Figure 18 shows the total sun reflected daily for the simulation period for January 1st to January, 31st, 2021, it was observed that the highest sun reflected was 304 degree obtained at January 30th, 2021, while the lowest was 173 degree obtained at 31st January, 2021. Figure 4.14-4.16 shows the simulation done in Helioclim-3 for the different tilt angle 300, 600 and 900, used in generating the data used to generate predictive models.

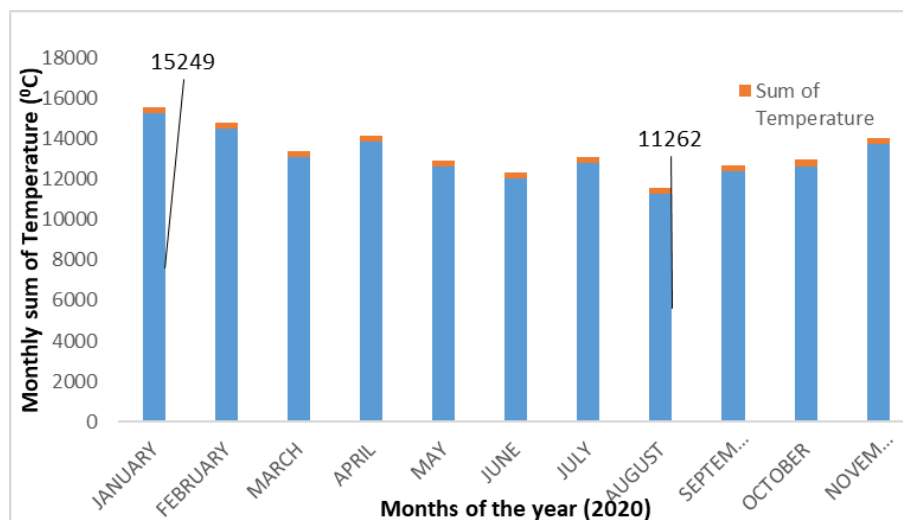


Figure 16: Sum of monthly temperature and reflected

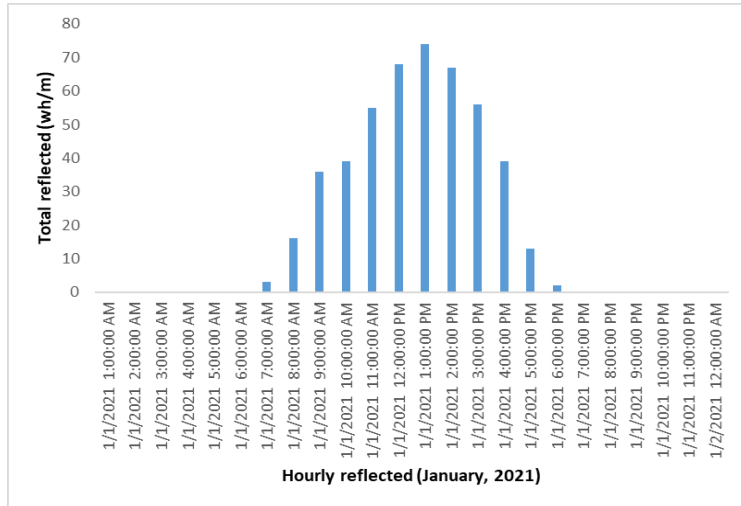


Figure 17: Hourly sun time graph for January,2021

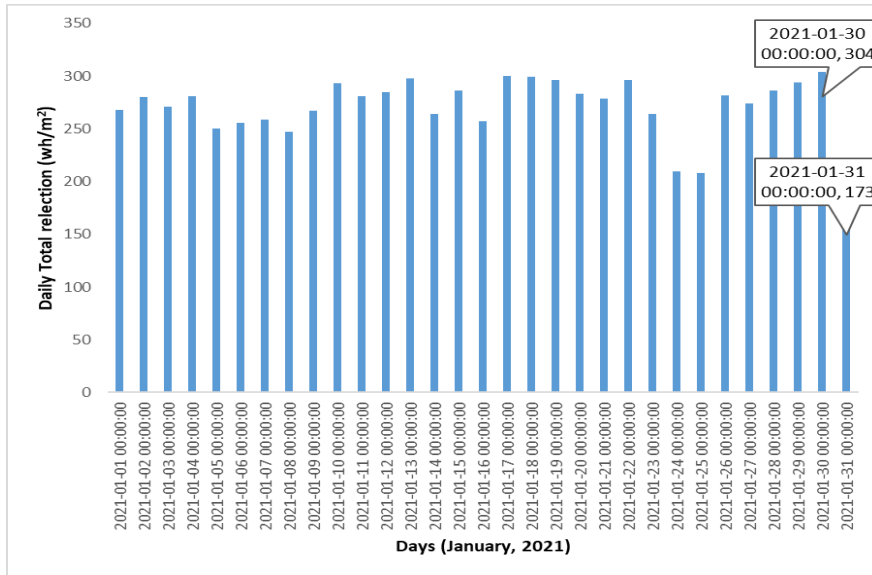


Figure 18: Total reflected sun for January 1st-January, 31st, 2021

Figure 19: Helioclim simulation for 30 degree tilt angle

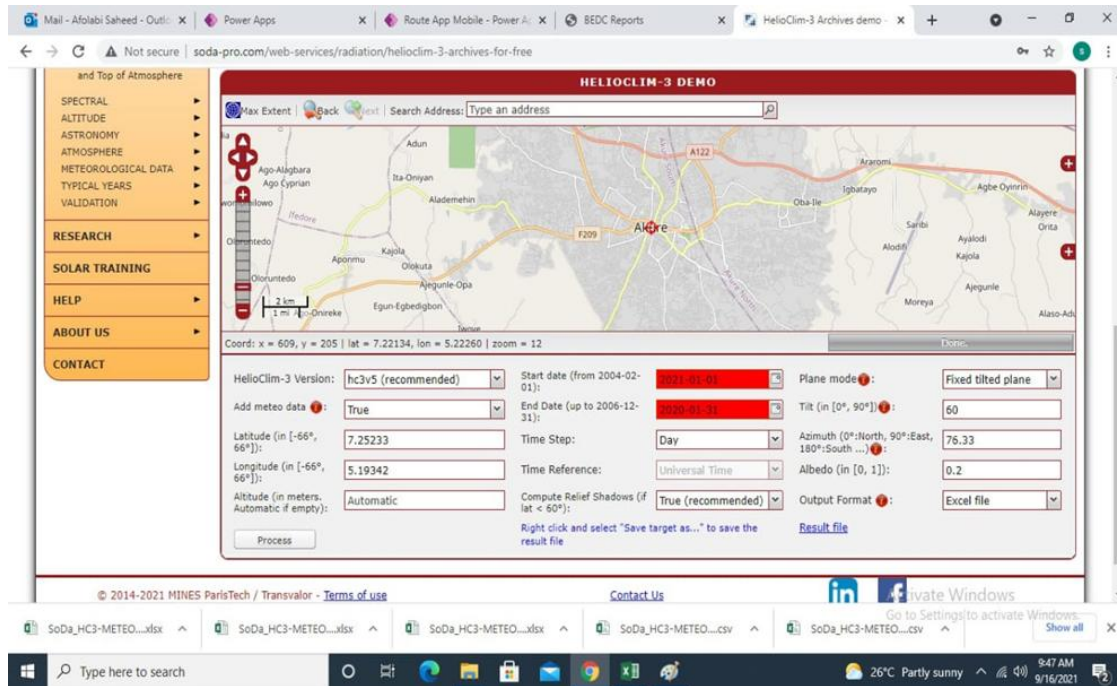


Figure 20: Helioclim simulation for 60 degree tilt angle

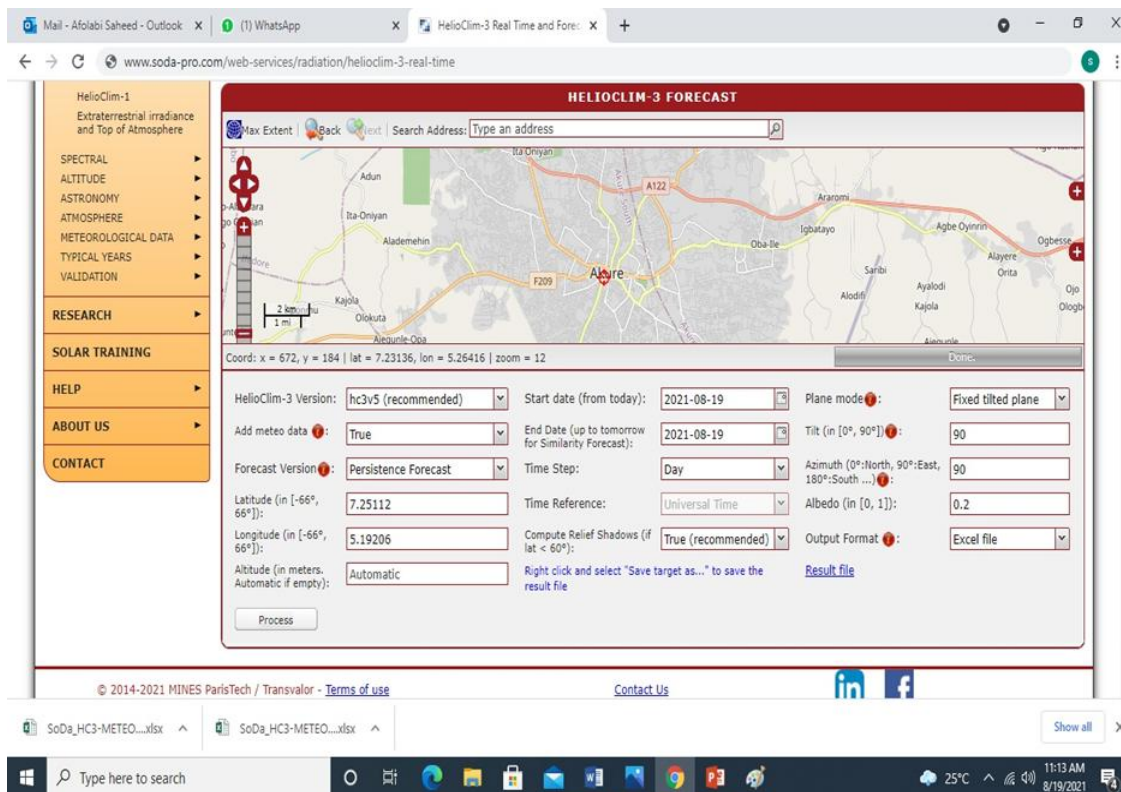


Figure 21: Helioclim simulation for 90degree tilt angle

Predictive Model Formulation Irradiance

The result for the model generated for irradiance is as shown in Table 5, it was observed that the Model F-value of 0.56, which implies that the model is significant relative to the interaction between the factors and response. There is a 19.73% chance that an F-value this large could occur due to interaction. The P-values less than 0.0500 indicate model terms are significant. Which agrees with Emmanuel et al. (2014) that found out that the values obtained in lower interval ($p < 0.05$) are more accurate than that of the higher interval. In this case there is one significant model terms. It was observed that wind has significant effect on the irradiance generated with p-value of 0.0319, while

others are not significant, this means that wind is an important factor that can cause deformation which agrees with the heliostat designed by Wang and Li (2012), revealing that wind has significant which should have a good agreement with experimental and numerical works. Since there are two values greater than 0.1000, it indicates that the model terms are significant. If there are many insignificant model terms (not counting those required to support hierarchy), model reduction may improve the model.

The Lack of Fit F-value of 1.60 implies the Lack of Fit is not significant relative to the pure error. There is a 10.55% chance that a Lack of Fit F-value. This large value of lack of fit could occur due to factors like temperature, tilt angle and day time. Non-significant lack of fit is good; the model has a linear fit has shown in Equation 27.

$$\text{Irradiance} = -26.2997 + 0.0736903 * A - 2.60408 * B - 0.389386 * C + 0.112571 * D \quad (27)$$

$$R^2 = 0.8690$$

where, A is the tilt angle, B is daytime, C is wind and D is temperature

The Predicted coefficient of determination (R^2) of 0.8690 is not as close to the Adjusted R^2 of 0.3781 as it might normally be expect, i.e. the difference is more than 0.5 as shown in Table 6. This may indicate a large block effect or a possible problem with your model and/or data. Things to consider are model reduction, response transformation, outliers, etc. All empirical models should be tested by doing confirmation runs. Adequate precision measures the signal to noise ratio. A ratio greater than 4 is desirable. The ratio of 6.498 indicates an adequate signal. This model can be used to navigate the design space. Figure 22 shows the validation of the model using the observed data against the predicted one, the validation gives almost the same R^2 value of 0.9001 which is good for the model.

The code was written in R language to generate a graphic user interface (GUI) for calculating irradiance has seen in Figure 23 and 24.

Table 5: Effect of tilt angle, daytime, wind and temperature on irradiance

Response 1: Irradiance

Source	Sum of Squares	df	Mean Square	F-value	p-value	
Model	505.01	4	126.25	0.56	0.0319	significant
A-tilt angle	302.31	1	302.31	3.74	0.1382	not significant
B-day time	104.87	1	104.87	1.30	0.2597	not significant
C-wind	50.70	1	50.70	0.6266	0.0319	significant
D-temperature	47.14	1	47.14	0.5826	0.4484	not significant
Residual	4611.84	57	80.91			
Lack of Fit	2139.68	20	106.98	1.60	0.1055	not significant
Pure Error	2472.17	37	66.82			
Cor Total	5116.85	61				

Table 6: Fit Statistics for the irradiance model

Fit Statistics for the irradiance model			
Std. Dev.	34.61	R^2	0.8690
Mean	24.24	Adjusted R^2	0.3781
C.V. %	142.77	Predicted R^2	0.0690
		Adeq Precision	6.4977

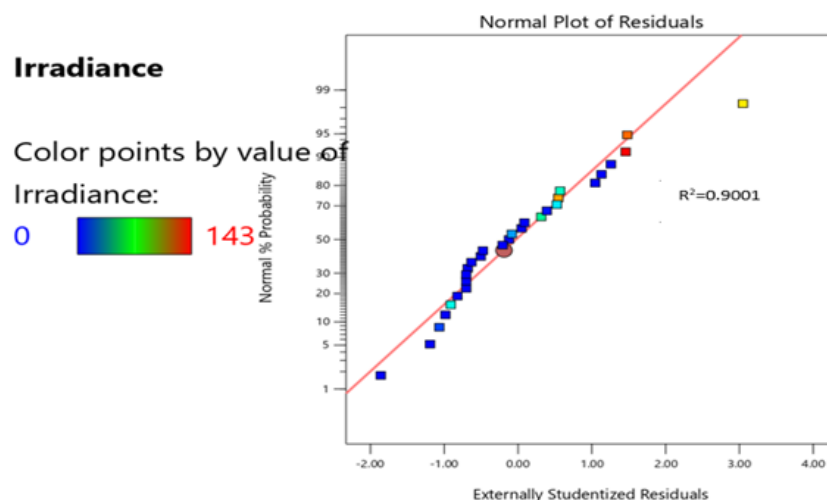


Figure 22: Validation of the irradiance Model

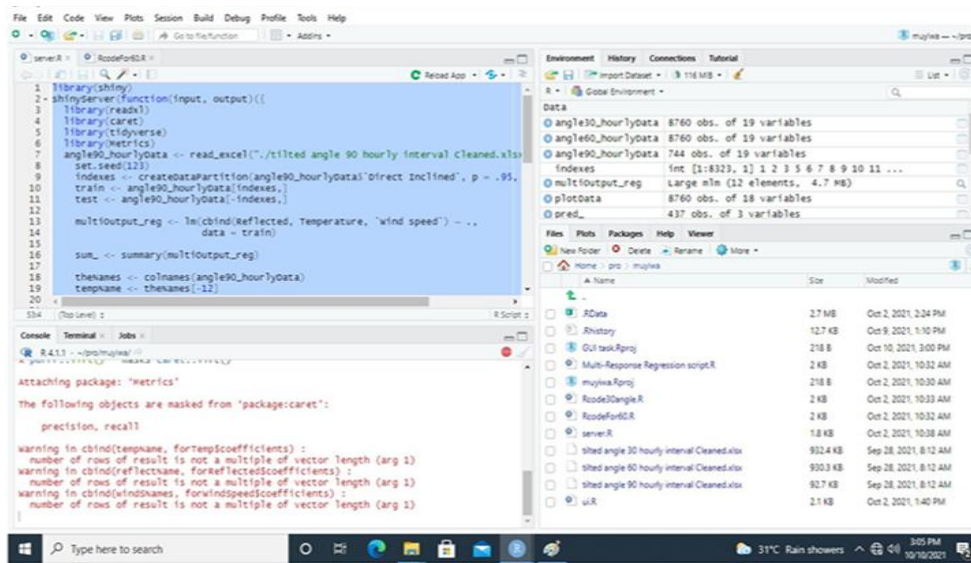


Figure 23: Code written R language

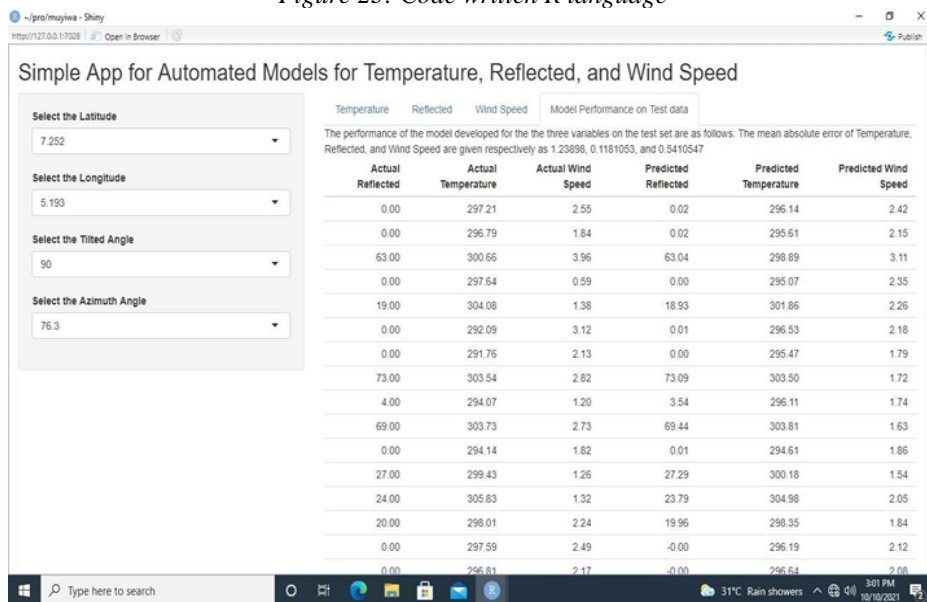


Figure 24: Graphic user interface produced from R programming

CONCLUSION

This study has presented a detailed heliostat design procedure and simulation with the interaction of these principles to generate steam with experimental period from 1st January - 31st January, 2021. The designed heliostat field plot has total reflective area of 50 m² and uses 1 units of single-axis heliostats. This study has provided the coordinates, facing and target angle for the heliostat in the proposed field. According to stress simulations, the maximum, 1st and 3rd principal stress acting on the heliostat was 7.28 MPa and 0.61 MPa, while maximum displacement was 20.39 mm, this means that deformation caused by stress would be small. The tower where the water was to be was also simulated and there is a need to add some reinforce especially at the base. The designed heliostat wind load calculated compared to the simulated wind at different degree shows the facet and the whole structure would not fail. The ray tracing for the mirror facet was able to generate good flux density which informs that it has good reflective potential. The predictive linear model for irradiance has R² value of 0.8960 with its validation value of 0.9001. The developed interface can be used to predict the required heat generated on a single facet heliostat to generate steam.

REFERENCES

[1]. Burgess G., Shortis, M., Kearton, A. and Garzoli. J. (2009). "Photogram try for dish concentrator construction". Solar09, 46th ANZSES Conference, Townsville, 3:29-39.
 [2]. Capecchi, D. and Ruta, G. (2015). The Theory of Elasticity in the 19th Century.

-
- [3]. Emmanuel, G., Ivo, A., Jesus, B., Jean, L. S. and Christian, W. (2014). "Comparison of 3 heat flux gauges and a water calorimeter for concentrated solar irradiance measurement", *Energy Procedia*, 49 pp. 2090 – 2099.
 - [4]. Garcia, P., Ferriere, A. and Bezian, J. J. (2008). Codes for solar flux calculation dedicated to central receiver system applications: A comparative review. *Solar Energy*, 82(3): p. 189-197.
 - [5]. Ghanadi, F., Yu, J., Emes, M., Arjomandi, M., Kelso, R., (2016). Numerical Investigation of Wind Loads on an Operating Heliostat, *SolarPACES 2016 conference*, in press.
 - [6]. Griffith, D. T., Moya, A. C., Ho, C. and Hunter, P. S. (2011). Structural dynamics testing and analysis for design evaluation and monitoring of heliostats. In *Proceedings of the 5th International Conference on Energy Sustainability, ES2011-54222*, pp. 567-576, ASME, Washington, DC.
 - [7]. Ho, C., Griffith, D. T., Sment, J., Moya, A. C., Christian, J. M., Yuan, J. K. and Hunter, P. S. (2012). Dynamic testing and analysis of heliostats to evaluate impacts of wind on optical performance and structural fatigue, *Proceedings of Solar Power and Chemical Energy Systems (SolarPACES) 2012 Conference, Marrakech, Morocco*. pp. 240-258
 - [8]. Huss, S., Traeger, Y. D., Shvets, Z., Rojansky, M., Stoyanov, S. and Garber, J., (2011). Evaluating effects of wind loads in heliostat design. In *Proceedings of the 17th SolarPACES International Conference, Granada, Spain*. pp. 202-220.
 - [9]. Jia, Y., Alva, G., and Fang, G. (2019). Development and applications of photovoltaic–thermal systems: A review. *Renewable and Sustainable Energy Reviews*, 102, 249-265.
 - [10]. Khodayar Sahebi H, Hoseinzadeh S, Ghadamian H, Ghasemi MH, Esmailion F, Garcia DA. (2021). Techno-Economic Analysis and New Design of a Photovoltaic Power Plant by a Direct Radiation Amplification System. *Sustainability*. 13(20):11493. <https://doi.org/10.3390/su132011493>
 - [11]. Ochsner, R, Stephen H, Koin E, Ajay Chandak, B, Kevin A, Patricia M, Tom C, Susan K, and Jesse D (2015). "News You Send." *Solar Cooker Review* 16 (Apr. 2010): n. pag. *Solar Cookers International*. Web. 02 Feb. 2015.
 - [12]. Okeniyi, J. M, Elizabeth, I. O. (2015). Wind characteristics and energy potential assessment in Akure, South West Nigeria: econometrics and policy implications. *International Journal of Ambient Energy*. 36. 282–300. 10.1080/01430750.2013.864586.
 - [13]. Peterka, D. (1992). Wind load design methods for ground-based heliostats and parabolic dish collectors. Fort collins, CO, USA: Sandia National Laboratories.
 - [14]. Peterka, J.A. and Derickson, R.G. (1992). Wind Load Design Methods for Ground-Based Heliostats and Parabolic Dish Collectors. Tech. Rep. SAND92-7009, Sandia National Laboratories, Albuquerque, NM.
 - [15]. Philibert, C. (2005). "The Present and Future Use of Solar Thermal Energy as a Primary Source of Energy", Copyright 2005 by Inter Academy Council All Rights Reserved. 12, 13-27.
 - [16]. Rashid, M.S.R.B.M.; Zheng, J.; Sng, E.; Rajendhiran, K.M.; Ye, Z.; Lim, L.H.I. (2021). An enhanced cloud segmentation algorithm for accurate irradiance forecasting. *Solar Energy*, 221, 218–231
 - [17]. Sukhatme, G. and Nayak, K. (2012). *Solar Energy: Principles of Thermal Collection and Storage*, Third Edition. New Delhi: Narosa Publishing House, pp. 200-222
 - [18]. Wang, Y., and Li, Z.N. (2012). Research on Numerical Simulation of Heliostat's Surface Wind Pressure. *Key Engineering Materials*, 517, 809 - 816.